

Article

Coordination Compounds of Nickel(II) with 3,5-Dibromo-Salicylaldehyde: Structure and Interaction with Biomolecules

Georgios I. Psarras , Ariadni Zianna , Antonios G. Hatzidimitriou and George Psomas * 

Department of General and Inorganic Chemistry, Faculty of Chemistry, Aristotle University of Thessaloniki, GR-54124 Thessaloniki, Greece

* Correspondence: gepsomas@chem.auth.gr

Abstract: Three neutral nickel(II) complexes of 3,5-dibromo-salicylaldehyde (3,5-diBr-saloH) were synthesized in the presence or absence of 1,10-phenanthroline (phen) or its derivative 2,9-dimethyl-1,10-phenanthroline (neoc) as co-ligands, namely [Ni(3,5-diBr-salo)₂(neoc)] (complex 1), [Ni(3,5-diBr-salo)₂(phen)] (complex 2) and [Ni(3,5-diBr-salo)₂(H₂O)₂] (complex 3), and were characterized by various techniques. The crystal structure of [Ni(3,5-diBr-salo)₂(neoc)] was determined by single-crystal X-ray crystallography. According to employed studying techniques, the complexes interact tightly with calf-thymus DNA by an intercalative fashion. Furthermore, compounds 1–3 bind tightly and reversibly to human and bovine serum albumin.

Keywords: nickel(II) complexes; 3,5-dibromo-salicylaldehyde; phenanthroline; DNA-interaction; affinity for albumins



Citation: Psarras, G.I.; Zianna, A.; Hatzidimitriou, A.G.; Psomas, G. Coordination Compounds of Nickel(II) with 3,5-Dibromo-Salicylaldehyde: Structure and Interaction with Biomolecules. *Inorganics* **2024**, *12*, 138. <https://doi.org/10.3390/inorganics12050138>

Academic Editors: Tamara Topala, Luminita Simona Oprean and Andreea Elena Bodoki

Received: 17 April 2024

Revised: 2 May 2024

Accepted: 7 May 2024

Published: 10 May 2024



Copyright: © 2024 by the authors. Licensee MDPI, Basel, Switzerland. This article is an open access article distributed under the terms and conditions of the Creative Commons Attribution (CC BY) license (<https://creativecommons.org/licenses/by/4.0/>).

1. Introduction

In medicinal chemistry, the quest for novel drugs is directed towards the synthesis and evaluation of either novel organic compounds that will operate as potential drugs or novel metal-based compounds incorporating (potentially) biologically active compounds as ligands [1,2]. An interesting group of bioactive molecules are the derivatives of salicylaldehyde. Salicylaldehyde or 2-hydroxy-benzaldehyde (saloH) is an organic compound found in the defensive secretion of some leaf beetle species [3]. Salicylaldehyde-based compounds are derivatives of saloH formed either by reactions through the carbonyl group leading to novel classes of compounds bearing the salicylaldehyde scaffold, such as Schiff bases [4–7], hydrazides [8,9], hydrazones [10–13], or thiosemicarbazones [14–16], or by the insertion of diverse substituents on one or more positions of the aromatic leading to substituted salicylaldehydes.

Halogens, nitro, alkyl, and alkoxy groups are the most common substituents (X) on the aromatic ring of salicylaldehydes leading to the formation of mono-substituted (X-saloH) or di-substituted salicylaldehydes (diX-saloH). Such modifications on the aromatic ring may alter the biological effect of the compounds [17,18]. In particular, the insertion of halogen substituents is important and may lead to ameliorated biological properties against bacteria and yeasts. It should be noted that halogen-containing compounds are almost 50% of the most active drugs [19] contributing to better membrane permeability [20]. 3,5-dibromosalicylaldehyde (3,5-diBr-saloH, Figure 1) is a dibromo-substituted salicylaldehyde which has been reported to inhibit the inositol-requiring enzyme 1, which may be related to the treatment of ischemic stroke [21,22].

Substituted salicylaldehydes can act as mono-, bi-, or even tri-dentate ligands when coordinating with metal ions and contribute to a wide spectrum of biological activity including DNA-interaction, albumin-binding, anticancer, antimicrobial, and antioxidant activity [19,23–27]. In the literature, the structures of diverse metal complexes with 3,5-dibromo-salicylaldehyde as ligand have been reported, including a series of mononuclear

zinc(II) [28] and copper(II) [29] complexes and a tetranuclear nickel(II) complex [30]. In addition, a mononuclear palladium(II) complex with 3,5-dibromo-salicylaldehyde was also evaluated for its biological activity [31].

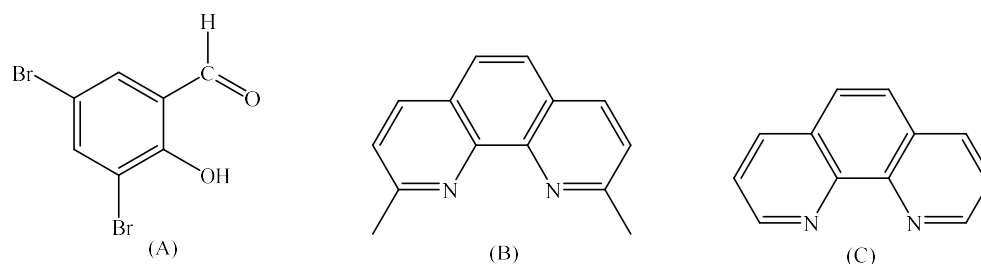


Figure 1. Syntax formula of (A) 3,5-dibromo-salicylaldehyde (3,5-diBr-saloH), (B) 2,9-dimethyl-1,10-phenanthroline (neoc), and (C) 1,10-phenanthroline (phen).

Nickel is an element involved in life evolution before the accumulation of oxygen [32]. However, the biological relevance of nickel is still significant [33,34], although nickel is deemed as dangerous for the health of nickel metallurgy workers [34–37] and responsible for diverse contact allergies related with nickel-coated jewelries and other routine objects [34,38]. Urease is an enzyme involved in the biological cycle of urea and is considered the most important nickel-bearing enzyme [33,34,39]. Nickel is also present in the active center of other metalloenzymes [32–34,40]. In modern bioinorganic chemistry, a significant number of nickel-based bioactive compounds have been reported [41,42] including examples presenting significant in vitro anticancer [43–45], antiepileptic [46], antifungal [47], anti-inflammatory [48], antimicrobial [49,50], and antioxidant [51–54] activity. In particular, nickel(II) complexes with substituted salicylaldehydes have recently gained an increasing interest regarding structural characterization and biological profile. More specifically, a plethora of mononuclear nickel(II) complexes with a series of substituted salicylaldehydes, such as the mono-substituted ones 5-chloro-salicylaldehyde, 5-bromo-salicylaldehyde, 5-fluoro-salicylaldehyde, 3-methoxy-salicylaldehyde, 5-methyl-salicylaldehyde, and 5-nitro-salicylaldehyde, and the di-substituted derivative 3,5-dichloro-salicylaldehyde, have been reported in the literature, and their interaction with biomacromolecules and antibacterial activity has been evaluated [55–57]. Furthermore, heterocubane-like nickel(II) complexes of dihalogen-substituted salicylaldehydes (i.e., 3,5-dichloro-salicylaldehyde, 3,5-iodo-salicylaldehyde, 3,5-dibromo-salicylaldehyde, and 3-bromo-5-chloro-salicylaldehyde) bearing the formula $[\text{Ni}_4(\text{diX-salo})_4(\mu_3\text{-OMe})_4(\text{MeOH})_4]$ have been recently reported by M. Aryaeifar et al. [30].

As a continuation of our research concerning metal complexes of substituted salicylaldehydes, three novel neutral mononuclear Ni(II) complexes of 3,5-diBr-saloH in the presence or absence of the *N,N'*-donors 2,9-dimethyl-1,10-phenanthroline (neocuproine, neoc) and 1,10-phenanthroline (phen) (Figure 1), formulated as $[\text{Ni}(3,5\text{-diBr-salo})_2(\text{neoc})]$ (complex 1), $[\text{Ni}(3,5\text{-diBr-salo})_2(\text{phen})]$ (complex 2) and $[\text{Ni}(3,5\text{-diBr-salo})_2(\text{H}_2\text{O})_2]$ (complex 3), were synthesized. The characterization of complexes 1–3 was afforded by physicochemical and spectroscopic (FT-IR and UV-vis) techniques. In addition, the molecular structure of $[\text{Ni}(3,5\text{-diBr-salo})_2(\text{neoc})]$ was determined by single-crystal X-ray crystallography. The interaction of compounds 1–3 with calf-thymus (CT) DNA was evaluated by DNA viscosity measurements and UV-vis spectroscopy titration studies, and through the ability to replace ethidium bromide (EB) in the EB-DNA adduct. The affinity of the compounds for bovine serum albumin (BSA) and human serum albumin (HSA) was monitored by fluorescence emission spectroscopy, and the corresponding binding constants were calculated.

2. Results

2.1. Synthesis and Characterization

Complexes 1–3 were efficiently synthesized in methanol through the aerobic reaction of $\text{NiCl}_2 \cdot 6\text{H}_2\text{O}$ with the sodium salt of 3,5-dibromo-salicylaldehyde (generated in situ by

the addition of CH_3ONa) in the presence or absence of the N,N' -donors. In all cases, a 1:2 $\text{Ni}^{2+}:(3,5\text{-diBr-salo}^-)$ ratio was employed, while for complexes **1** and **2**, the corresponding N,N' -donor (neoc, phen) was added in a 1:2:1 $\text{Ni}^{2+}:(3,5\text{-diBr-salo}^-):(N,N'\text{-donor})$ ratio (Figure 2). The characterization of the resulting complexes **1–3** was achieved through physicochemical and spectroscopic techniques (FT-IR and UV-vis), and, especially for complex **1**, by single-crystal X-ray crystallography.

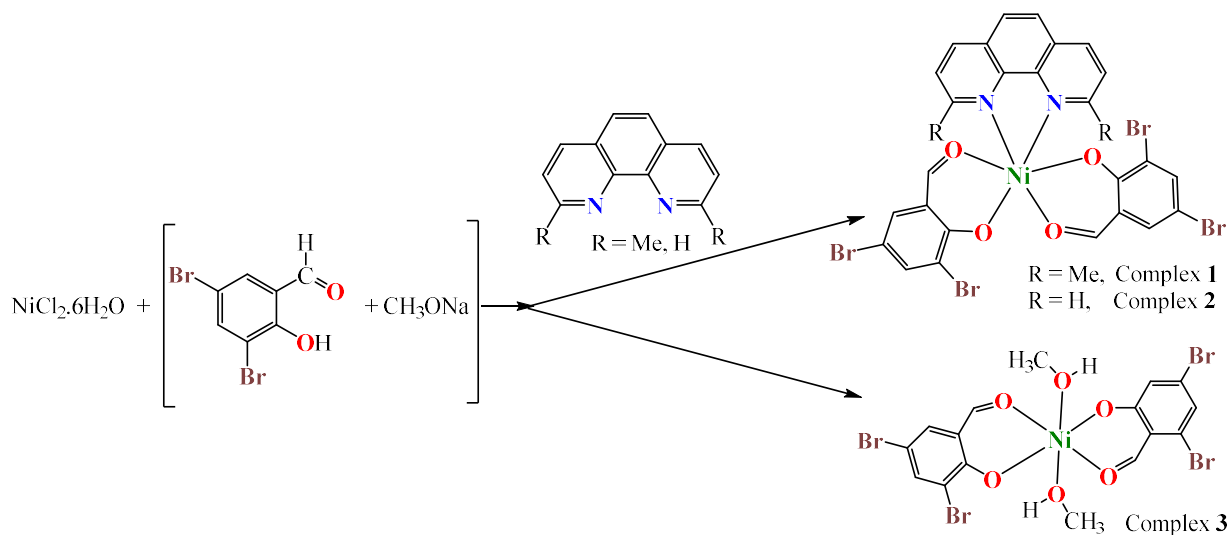


Figure 2. Synthetic routine and proposed structures for complexes **1–3**.

According to the molar conductivity values of the complexes in 1 mM of DMSO solution found in the range $10\text{--}15 \text{ mho} \cdot \text{cm}^2 \cdot \text{mol}^{-1}$, complexes **1–3** are neutral in nature [58], possessing a 1:2:1 $\text{Ni(II)}:(3,5\text{-diBr-salo}^-):(N,N'\text{-donor})$ composition (complexes **1** and **2**) or a 1:2 $\text{Ni(II)}:(3,5\text{-diBr-salo}^-)$ composition (complex **3**). Room-temperature (RT) magnetic measurements performed for complexes **1–3** derived μ_{eff} values in the range 2.90–3.00 BM, which were slightly higher than the RT spin-only values ($=2.83 \text{ BM}$) and confirmed the mononuclear nature of the complexes in solid state [33]. These data were also confirmed by elemental analyses data and were in good agreement with the suggested molecular formulas.

The FT-IR spectra (Figure S1) confirmed the deprotonation and the coordination mode of 3,5-dibromo-salicylaldehyde, as well as the presence of the N,N' -donor co-ligands in the complexes (complexes **1** and **2**). In the IR spectrum of free 3,5-diBr-saloH, the sharp bands located at $\sim 3200 \text{ cm}^{-1}$ and $\sim 1400 \text{ cm}^{-1}$ are assigned to the vibrations of the phenolic $-\text{OH}$. The first band disappears in the spectra of the complexes, indicating the deprotonation of the salicylaldehyde, while the second one is shifted towards $1315\text{--}1340 \text{ cm}^{-1}$, implying the coordination through the phenolic oxygen ($\text{C}-\text{O} \rightarrow \text{Ni}$). The band at 1679 cm^{-1} attributed to the $\nu(\text{C}=\text{O})$ in the free 3,5-diBr-saloH [28,29] is shifted to lower wavenumbers ($1622\text{--}1647 \text{ cm}^{-1}$), revealing its coordination with the metal through the carbonyl oxygen [59]. For complexes **1** and **2**, the band attributed to the characteristic out-of-plane $\rho(\text{C}-\text{H})$ vibrations of the N,N' -donor ligand is observed at 726 cm^{-1} and 732 cm^{-1} , respectively [59].

The electronic spectra of complexes **1–3** were recorded both in solid state (in the form of nujol mull) and in DMSO solution (and over time intervals spanning up to three days) in order to evaluate their stability in solution and during time (Figures S2 and S3). For the solution investigations, the complexes were dissolved either in DMSO or a DMSO:buffer (150 mM of NaCl and 15 mM of trisodium citrate, $\text{pH} = 7$) mixture. In the visible region of the spectra of complexes **1–3** in DMSO, three bands attributed to d-d transitions were located at 1025–1040 nm ($\epsilon = 5\text{--}10 \text{ M}^{-1}\text{cm}^{-1}$), 630–670 nm ($\epsilon = 25\text{--}70 \text{ M}^{-1}\text{cm}^{-1}$), and 420–422 nm ($\epsilon = 1260\text{--}1300 \text{ M}^{-1}\text{cm}^{-1}$) and may be assigned to ${}^3\text{A}_{2g} \rightarrow {}^3\text{T}_{2g}$, ${}^3\text{A}_{2g} \rightarrow {}^3\text{T}_{1g}(\text{F})$ and ${}^3\text{A}_{2g} \rightarrow {}^3\text{T}_{1g}(\text{P})$ transitions, respectively [33]. These three d-d bands are characteristic for octahedral nickel(II) complexes [33]. The values of 10Dq and the Racah B parameters were also determined. The existence of these bands attributed to d-d transitions as well as the

values of the ratio $10Dq/B$ (which were calculated in the range 14.0–15.5) are characteristic for distorted octahedral Ni^{2+} complexes [33,57,60].

The overall behavior of complexes **1–3** in solution (the similarity with electronic spectra in solid state and the non-electrolytic nature according to the molar conductivity measurements) serves also as evidence of their stability in solution.

2.2. Structure of the Complexes

Among the complexes under study, single-crystals were obtained only for $[Ni(3,5\text{-diBr-salo})_2(\text{neoc})]$ (complex **1**), and the molecular structure was determined by single-crystal X-ray crystallography. The experimental X-ray crystallography details for this compound are summarized in Table 1. Complex **1** crystallized in the monoclinic crystal system and $P2_1/c$ space group. The molecular structure of the complex is depicted in Figure 3, and selected bond lengths and angles are summarized in Table 2.

Table 1. Experimental X-ray crystallography details for $[Ni(3,5\text{-diBr-salo})_2(\text{neoc})]$ (complex **1**).

Complex 1	
Crystal data	
Chemical formula	$C_{28}H_{18}Br_4N_2NiO_4$
M_r	824.79
Crystal system	Monoclinic
Space group	$P2_1/c$
Temperature (K)	295
a (Å)	16.604 (8)
b (Å)	24.002 (13)
c (Å)	14.571 (8)
β (°)	103.381 (12)
V (Å ³)	5649 (5)
Z	8
Radiation type	Mo $K\alpha$
μ (mm ⁻¹)	6.38
Crystal size (mm)	0.15 × 0.12 × 0.11
Data collection	
Diffractometer	Bruker Kappa Apex2
Absorption correction	Numerical Analytical Absorption (De Meulenaer and Tompa, 1965)
T_{min}, T_{max}	0.46, 0.50
No. of measured reflections	58,802
No. of independent reflections	10,738
No. of observed [$I > 2.0\sigma(I)$] reflections	7018
R_{int}	0.042
$(\sin \theta / \lambda)_{max}$ (Å ⁻¹)	0.613
Refinement	
$R[F^2 > 2\sigma(F^2)]$	0.038
$wR(F^2)$	0.085
S	1.00
No. of reflections	7018
No. of parameters	703
H-atom treatment	H-atom parameters constrained
$\Delta\rho_{max}, \Delta\rho_{min}$ (e Å ⁻³)	0.49, -0.98

The asymmetric unit of complex **1** contains two crystallographically independent complex molecules notated as A and B, i.e., **1A** and **1B**, respectively. In both complexes, the 3,5-diBr-salo⁻ ligands are deprotonated and coordinate bidentately to Ni(II) ions through the phenolato oxygens (O2 and O4 in **1A**; O6 and O8 in **1B**) and the aldehyde (O1 and O3 in **1A**; O5 and O7 in **1B**) oxygen atoms forming six-membered chelate rings (the chelate $O_{phenolato}\text{-Ni-O}_{aldehyde}$ angles are in the range 86.99(16)–89.41(17)°).

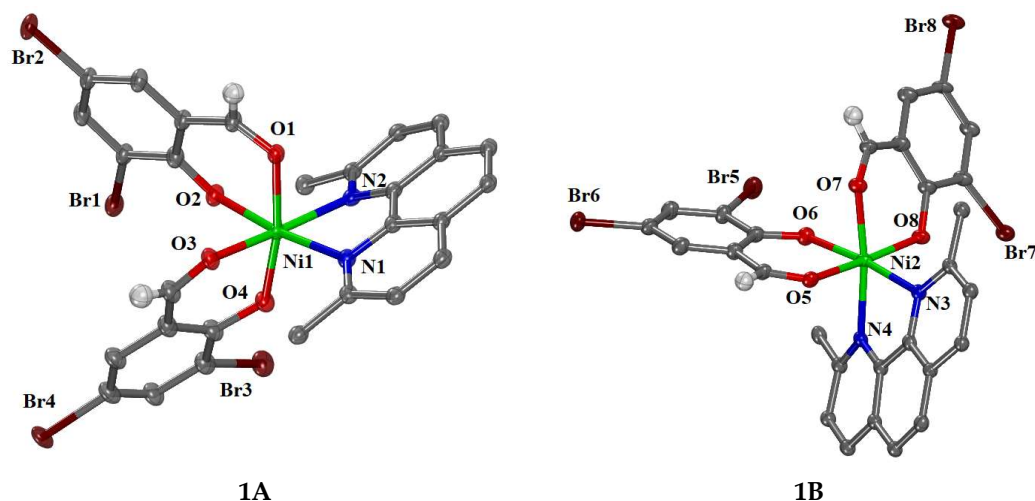


Figure 3. Molecular structure of $[\text{Ni}(\text{3,5-diBr-salo})_2(\text{neoc})]$ (complex **1**). Aromatic hydrogen and methyl hydrogen atoms have been omitted for clarity.

Table 2. Selected bond lengths (Å) and bond angles (°) for $[\text{Ni}(\text{3,5-diBr-salo})_2(\text{neoc})]$ (complex **1**).

1A		1B	
Bond	Length (Å)	Bond	Length (Å)
Ni1—O1	2.106(4)	Ni2—O5	2.092(4)
Ni1—O2	2.018(4)	Ni2—O6	2.033(4)
Ni1—O3	2.097(5)	Ni2—O7	2.060(4)
Ni1—O4	1.953(4)	Ni2—O8	2.037(4)
Ni1—N1	2.115(5)	Ni2—N3	2.134(5)
Ni1—N2	2.160(5)	Ni2—N4	2.103(5)
Bonds	Angle (°)	Bonds	Angle (°)
O1—Ni1—O2	86.99(16)	O5—Ni2—O6	89.41(17)
O1—Ni1—O4	170.44(17)	O5—Ni2—O8	173.40(18)
O2—Ni1—N1	173.05(19)	O6—Ni2—N3	172.78(17)
O3—Ni1—O4	87.93(19)	O7—Ni2—O8	88.58(17)
O3—Ni1—N2	172.04(17)	O7—Ni2—N4	171.09(17)
N1—Ni1—N2	78.3(2)	N3—Ni2—N4	78.54(19)

The Ni(II) ions are six-coordinate with a NiN_2O_4 chromophore and a distorted octahedral geometry. Four of the six vertices of the octahedron are occupied by the oxygen atoms of the 3,5-diBr-salo[−] ligands and the remaining two sites by the nitrogen atoms of the neoc ligand. In both complexes, the Ni—O_{phenolato} (1.953(4)–2.037(4) Å) are the shortest and the Ni—N_{neoc} (2.103(5)–2.160(5) Å) are the longest bond lengths in the coordination sphere. In both complexes (**1A** and **1B**), the corresponding oxygen atoms are lying at *cis* positions to each other ($\text{O}_{\text{phenolato}}\text{—Ni—O}_{\text{phenolato}} = 85.41(18)\text{--}86.70(16)^\circ$; $\text{O}_{\text{aldehyde}}\text{—Ni—O}_{\text{aldehyde}} = 85.80(18)\text{--}94.37(17)^\circ$).

Such *cis* arrangement of the phenolato and aldehyde oxygen atoms around the metal ion is the least often found in the crystal structures of complexes bearing the formula $[\text{M}(\text{X-salo})_2(\text{N,N}'\text{-donor})]$ reported so far. In addition to complex **1**, this arrangement has been observed in the structures of $[\text{Zn}(\text{3,5-diCl-salo})_2(\text{bipyam})]$ (3,5-diCl-saloH = 3,5-dichloro-salicylaldehyde; bipyam = 2,2'-bipyridylamine) [27], $[\text{Mn}(\text{5-NO}_2\text{-salo})_2(\text{phen})]$, and $[\text{Mn}(\text{5-NO}_2\text{-salo})_2(\text{bipy})]$ (5-NO₂-saloH = 5-nitro-salicylaldehyde; bipy = 2,2'-bipyridine) [61]. The most often case is the arrangement of the phenolato oxygen atoms in *trans* positions, as found in a series of Zn(II) [26,28,62], Cd(II) [63,64], and Co(II) [65–68] mononuclear complexes. Quite often found is the *trans* arrangement of the aldehyde oxygens, as reported in a series of Zn(II) [62], Mn(II) [24,61], Cd(II) [64], and Co(II) [68]

complexes. It should also be noted that complex **1** is the first neutral Ni(II) complex bearing $X\text{-salO}^-$ and N,N' -donor ligands that is structurally characterized by X-ray crystallography; till now, the reported crystal structures refer to cationic Ni(II) complexes of the general formula $[\text{Ni}(X\text{-salO})(N,N'\text{-donor})_2]^+$ [55–57].

From the experimental data collected from elemental analysis, RT magnetic and Λ_M measurements, infrared and electronic spectroscopies, and from a comparison with similar reported crystal structures, the structures for complexes **2** and **3** may be proposed (Figure 2). In both compounds, the deprotonated 3,5-diBr-salO[−] ligands are coordinated to Ni(II) ions in a bidentate mode through the aldehyde and phenolato oxygen atoms. In complex **2**, a NiN₂O₄ coordination sphere is expected around Ni(II) formed by two bidentate 3,5-diBr-salO[−] ligands and a bidentate phen ligand leading to a structure (Figure 3) similar to that of complex **1** and other reported complexes with formula $[\text{M}(X\text{-salO})_2(N,N'\text{-donor})]$ [24,26–28,61,62]. On the other hand, complex **3** is expected to have a NiO₆ coordination sphere originated from the coordination of two bidentate 3,5-diBr-salO[−] and two methanol ligands and a structure (Figure 2) similar to those reported for complexes $[\text{Ni}(3,5\text{-diCl-salO})_2(\text{H}_2\text{O})_2]$ [57], $[\text{Ni}(5\text{-Cl-salO})_2(\text{CH}_3\text{OH})_2]$ (5-Cl-salOH = 5-chloro-salicylaldehyde), and $[\text{Ni}(5\text{-Br-salO})_2(\text{CH}_3\text{OH})_2]$ (5-Br-salOH = 5-bromo-salicylaldehyde) [56].

2.3. Interaction of the Complexes with CT DNA

Coordination compounds can interact with linear DNA through either covalent (base-binding) or noncovalent mechanisms (intercalation, electrostatic interactions, groove-binding) or may induce cleavage in the DNA helix [69]. The interaction between complexes **1–3** and CT DNA was explored by UV-vis spectroscopy and viscosity measurements, and via their ability to displace EB for EB-DNA adduct, which was monitored by fluorescence emission spectroscopy.

UV-vis spectroscopy is used preliminarily to obtain information regarding the DNA-interaction of the complexes and to determine the corresponding DNA-binding constant (K_b). In the UV-vis spectra of complexes **1–3**, two main bands were located in the regions 277–278 nm and 422–425 nm. Upon addition of a CT DNA solution, these two bands exhibited a hypochromism and a hyperchromism, respectively, accompanied by a slight red shift in most cases (Figure 4, Table 3). These spectral changes are indicative of interaction between the complexes and CT DNA, although drawing a definitive conclusion for the type of this interaction is not feasible. Consequently, additional experiments, such as viscosity and EB-displacement studies, were undertaken to shed light on the DNA interaction mode of the complexes [70,71].

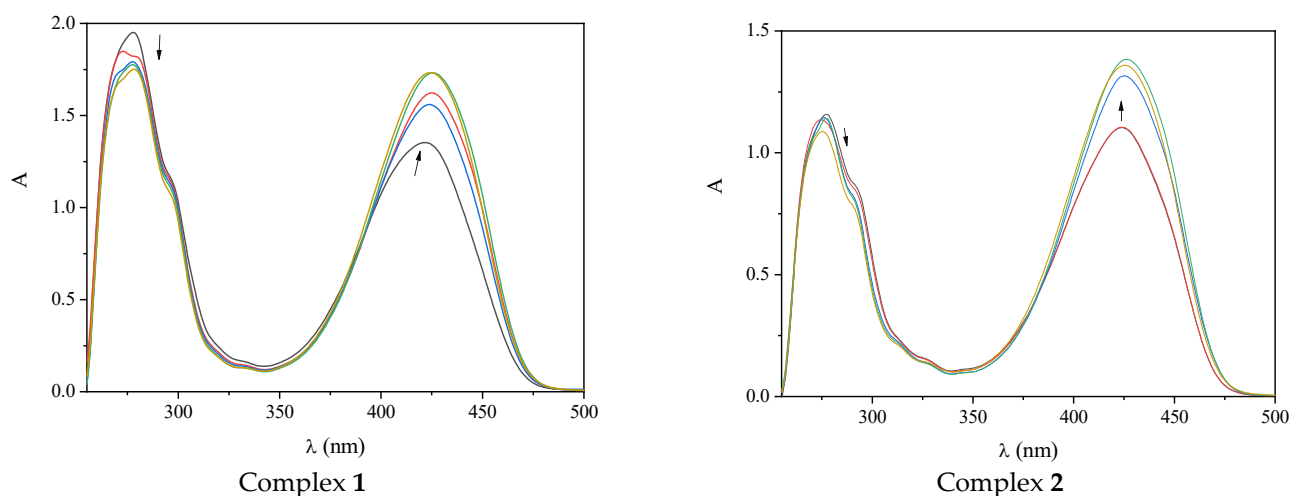


Figure 4. UV-vis spectra of a DMSO solution of $[\text{Ni}(3,5\text{-diBr-salO})_2(\text{neoc})]$ (complex **1**) and $[\text{Ni}(3,5\text{-diBr-salO})_2(\text{phen})]$ (complex **2**) (1×10^{-4} M) in the presence of increasing amounts of CT DNA. The arrows show the changes upon increasing amounts of CT DNA.

Table 3. UV–vis spectroscopic features of the interaction of 3,5-diBr–saloH and complexes 1–3 with CT DNA. UV band (λ_{\max} , nm) (percentage of the observed hyper-/hypo-chromism ($\Delta A/A_0$, %), red/blue shift ($\Delta\lambda$, nm)) and DNA-binding constants (K_b , in M^{-1}).

Compound	λ_{\max} (nm) (($\Delta A/A_0$, %) ^a ($\Delta\lambda$, nm) ^b)	K_b (M^{-1})
3,5-diBr–saloH [28]	337 (<-50 ^c , elim ^d), 427(>+50 ^c , 0)	$3.71(\pm 0.14) \times 10^5$
Complex 1	277 (-10, +1); 422 (+35, +3)	$4.22(\pm 0.86) \times 10^5$
Complex 2	277 (-8, 0); 425(+25, +4)	$3.26(\pm 0.75) \times 10^5$
Complex 3	278(-6, 0); 422 (+30, +3)	$2.83(\pm 0.70) \times 10^5$

^a “+” denotes hyperchromism; “-” denotes hypochromism. ^b “+” denotes red shift; “-” denotes blue shift. ^c “>+50” denotes intense hyperchromism; “<-50” denotes intense hypochromism. ^d “elim” denotes elimination of the band.

The DNA-binding constants of complexes 1–3 (K_b) were calculated with the Wolfe–Shimer equation (Equation (S1)) [72] and the corresponding plots of $[DNA]/(\epsilon_A - \epsilon_f)$ vs. $[DNA]$ (Figure S4). The calculated K_b values indicate a strong binding affinity of the complexes to DNA and are higher than that of the known intercalator EB ($K_b = 1.23 \times 10^5 M^{-1}$) [73], showing that complexes 1–3 may be tighter DNA-binders than EB. The DNA-binding constants of complexes 1–3 are in the range $2.83(\pm 0.70) \times 10^5$ – $4.22(\pm 0.86) \times 10^5 M^{-1}$ and are of the same magnitude with those calculated for a series of coordination compounds bearing substituted salicylaldehydes as ligands [24–28,57,61–64,74].

The DNA-interaction mode of the complexes was also evaluated by viscosity measurements. When a compound intercalates into the double DNA-helix, the nitrogen DNA-base pairs are separated, leading to an increase in DNA-length and, consequently, an increase in the DNA-viscosity. On the other hand, a compound interacting externally with DNA may cause DNA bending, leading to a slight decrease in DNA-length and, consequently, a slight decrease in DNA-viscosity. When a compound induces cleavage of a DNA-helix, much shorter fragments will be produced, resulting in a significant decrease in DNA-viscosity [75].

In the present case, the viscosity changes in a CT DNA solution (0.1 mM) were recorded in the presence of increasing amounts of complexes 1–3 (Figure 5). For complexes 1 and 2, the initial incremental addition (up to $r \sim 0.12$) resulted in a slight decrease in DNA-viscosity, thus suggesting an external approach to DNA. Further addition of the complexes ($r = 0.15$ – 0.36) resulted in an increase in the relative DNA-viscosity. For complex 3, the increase in DNA-viscosity was quicker and more pronounced than the other two complexes. The overall behavior of complexes 1–3 suggests that intercalation is their most probable mode of interaction with CT DNA [75].

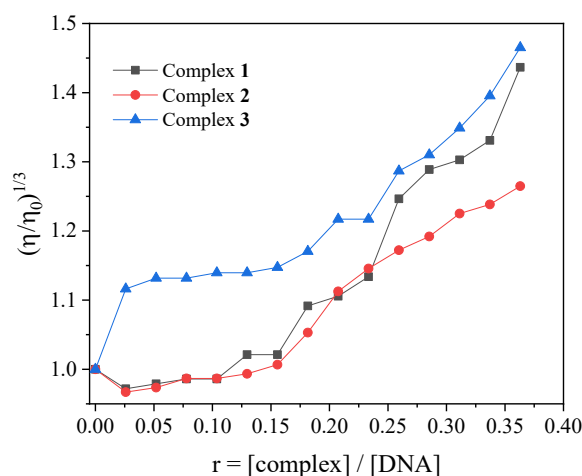


Figure 5. Relative viscosity $(\eta/\eta_0)^{1/3}$ of CT DNA (0.1 mM) in buffer solution (150 mM of NaCl and 15 mM of trisodium citrate at pH 7.0) in the presence of complexes 1–3 at increasing amounts ($r = [\text{complex}]/[\text{DNA}]$).

Ethidium bromide has the ability to fluoresce, especially when it intercalates in between a double DNA-helix via its planar phenanthridine ring. Given the known interaction mode of EB with DNA, EB is often used as a reference compound to study the interaction of potentially intercalating compounds [76]. The formed EB–DNA adduct presents a strong emission band at 594 nm, when excited at 540 nm. With the addition of a competitor of EB, this fluorescence emission intensity is quenched, assuming that the added compound does not fluoresce under similar conditions and may imply the displacement of EB by the added compound [76].

Solutions of complexes 1–3 were added incrementally in a pretreated solution containing the EB–CT DNA adduct (20 μM of EB, 26 μM of CT DNA), and the fluorescence emission spectra were recorded for each addition (Figure 6A). For all complexes, a quenching of the initial EB–DNA emission band at 594 nm was observed (up to 58.7% of the initial fluorescence was observed for complex 3, Figure 6B, Table 4) and was obviously assigned to the displacement of the EB from the preformed EB–DNA adduct by the complex under study.

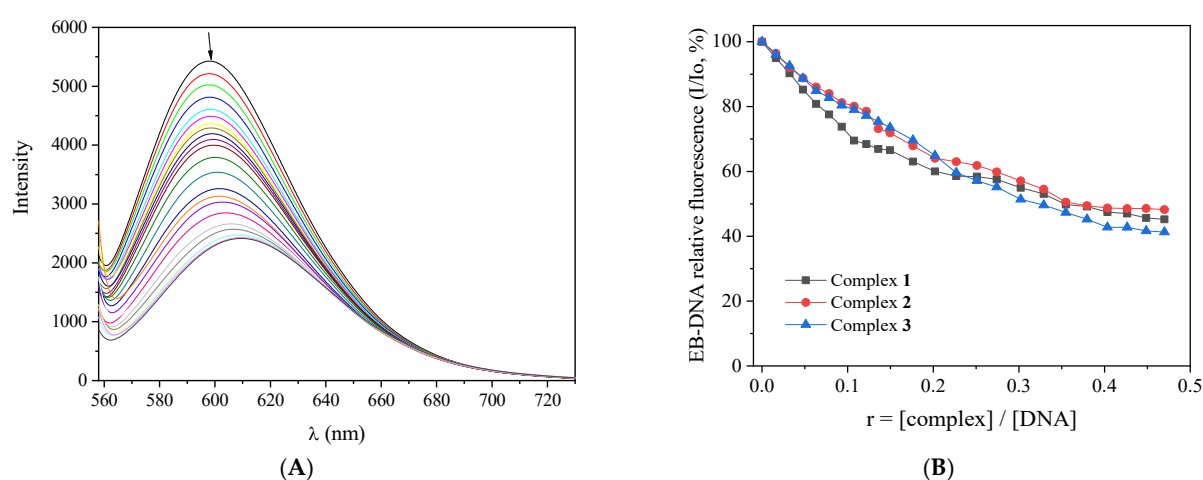


Figure 6. (A) Fluorescence emission spectra ($\lambda_{\text{excitation}} = 540 \text{ nm}$) for EB–DNA adduct ($[\text{EB}] = 20 \mu\text{M}$, $[\text{DNA}] = 26 \mu\text{M}$) in buffer solution (150 mM of NaCl and 15 mM of trisodium citrate at pH = 7.0) in the presence of increasing amounts of $[\text{Ni}(3,5\text{-diBr-salo})_2(\text{H}_2\text{O})_2]$ (complex 3). (B) Plot of relative EB–DNA fluorescence emission intensity at $\lambda_{\text{emission}} = 594 \text{ nm}$ (I/I_0 , %) vs. r ($r = [\text{complex}]/[\text{DNA}]$) in the presence of complexes 1–3 (up to 45.2% of the initial EB–DNA fluorescence for $[\text{Ni}(3,5\text{-diBr-salo})_2(\text{neoc})]$ (complex 1), 48.2% for $[\text{Ni}(3,5\text{-diBr-salo})_2(\text{phen})]$ (complex 2), and 41.3% for $[\text{Ni}(3,5\text{-diBr-salo})_2(\text{H}_2\text{O})_2]$ (complex 3)).

Table 4. Percentage of EB–DNA fluorescence quenching ($\Delta I/I_0$, %) and the Stern–Volmer (K_{SV} , in M^{-1}) and EB–DNA quenching constants (K_{q} , in $\text{M}^{-1}\text{s}^{-1}$) for 3,5–diBr–saloH and complexes 1–3.

Compound	$\Delta I/I_0$ (%)	K_{SV} (M^{-1})	K_{q} ($\text{M}^{-1}\text{s}^{-1}$)
3,5–diBr–saloH [28]	46.6	$3.95(\pm 0.10) \times 10^4$	$1.72(\pm 0.04) \times 10^{12}$
Complex 1	54.8	$4.11(\pm 0.11) \times 10^4$	$1.78(\pm 0.05) \times 10^{12}$
Complex 2	51.8	$8.56(\pm 0.15) \times 10^4$	$3.72(\pm 0.06) \times 10^{12}$
Complex 3	58.7	$5.33(\pm 0.09) \times 10^4$	$2.32(\pm 0.04) \times 10^{12}$

The Stern–Volmer constant (K_{SV}) and the quenching constant (K_{q}) of complexes 1–3 were calculated with the Stern–Volmer equations (Equations (S2) and (S3)) and the corresponding Stern–Volmer plots (Figure S5). The complexes present relatively high K_{SV} values which reveal their potency to displace EB from the EB–DNA adduct in order to bind tightly to DNA. The K_{q} values were calculated with Equation (S3) [76] using the value of 23 ns as the fluorescence lifetime of EB–DNA (τ_0) [77] and are within the range reported for other metal complexes containing X–salo as ligands [24–28,57,61–64,74]. All complexes exhibited quenching constants higher than the value of $10^{10} \text{ M}^{-1}\text{s}^{-1}$, implying the presence of a static

quenching mechanism for their interaction with the EB–DNA adduct, which indicates the formation of a new adduct between DNA and the complexes under study, and confirms indirectly intercalation as the most possible mode of interaction.

2.4. Interaction of the Complexes with Albumins

Serum albumins (SAs) play a crucial role, being the major proteins in the bloodstream of mammals. Their main function is to act as carriers for drugs and metal ions, facilitating their transport to different biological targets (cells and tissues). HSA is characterized by a solitary tryptophan at position 214. In comparison, BSA is extensively examined due to its structural resemblance to HSA and features two tryptophan residues, Trp–134 and Trp–212 [78,79]. BSA and HSA are quite similar, as their tryptophan residues are responsible for the appearance of an intense fluorescence emission band at $\lambda_{\max} = 343$ nm and $\lambda_{\max} = 340$ nm, respectively, when excited at 295 nm. The decrease in the intensity of this emission band when interacting with another compound indicates changes in their secondary structure, which is due to the binding of the compound [76].

The fluorescence emission spectra of albumins (3 μ M) in buffer solution were recorded in the presence of incremental amounts of complexes 1–3 (Figure 7A,C). Upon addition of complexes 1–3, a significant decrease in the intensity of the bands was observed, which was more pronounced for BSA (Figure 7B,D), and indicates the interaction between BSA and HSA with the complexes [80]. For the quantitative studies, the spectra of free complexes 1–3 were recorded under the same conditions and were subtracted from the overall spectra. In addition, the inner-filter effect was evaluated with Equation (S4) [81], and it was found negligible to affect the measurements.

The interaction of complexes 1–3 with both albumins was further assessed with Stern–Volmer and Scatchard equations and plots (Figures S6–S9) in order to calculate the SA-quenching constants (K_q) and SA-binding constants (K), respectively. The values of K_q were calculated with the Stern–Volmer equation (Equations (S2) and (S3)) and plots (Figures S6 and S7) with $\tau_0 = 10^{-8}$ s [76] as the fluorescence lifetime of tryptophan in SAs and are summarized in Table 5. The K_q values for both albumins are much higher than the value of $10^{10} \text{ M}^{-1}\text{s}^{-1}$, indicating the existence of a static quenching mechanism [76], which confirms subsequently the interaction between the albumins and the complexes [80].

Table 5. Albumin-quenching constants (K_q , in $\text{M}^{-1}\text{s}^{-1}$) and albumin-binding constants (K , in M^{-1}) for 3,5–diBr–salOH and complexes 1–3.

Compound	$K_{q(\text{BSA})}$ ($\text{M}^{-1}\text{s}^{-1}$)	$K_{(\text{BSA})}$ (M^{-1})	$K_{q(\text{HSA})}$ ($\text{M}^{-1}\text{s}^{-1}$)	$K_{(\text{HSA})}$ (M^{-1})
3,5–diBr–salOH [28]	$1.63(\pm 0.02) \times 10^{14}$	$5.76(\pm 0.30) \times 10^6$	$5.08(\pm 0.15) \times 10^{13}$	$1.55(\pm 0.10) \times 10^6$
Complex 1	$1.20(\pm 0.10) \times 10^{13}$	$1.01(\pm 0.10) \times 10^5$	$8.72(\pm 0.21) \times 10^{12}$	$2.23(\pm 0.21) \times 10^4$
Complex 2	$3.43(\pm 0.70) \times 10^{13}$	$8.21(\pm 0.70) \times 10^4$	$1.62(\pm 0.15) \times 10^{13}$	$2.50(\pm 0.15) \times 10^4$
Complex 3	$8.97(\pm 0.50) \times 10^{12}$	$1.89(\pm 0.50) \times 10^5$	$6.00(\pm 0.23) \times 10^{12}$	$9.13(\pm 0.23) \times 10^4$

The values of K were calculated with the Scatchard equation (Equation (S5)) [82] and plots (Figures S8 and S9), revealing tight binding of complexes 1–3 with both albumins. The calculated K_q and K values of complexes 1–3 for both albumins (Table 5) are comparable with those reported for metal(II) complexes with substituted salicylaldehydes as ligands [23–29,57,61,74,83]. In addition, the binding of the complexes to the albumins may be considered tight and reversible, when the albumin-binding constants are compared with the average value ($K \sim 10^{15} \text{ M}^{-1}$) of the binding constants of avidin with various compounds; this is the known borderline value for noncovalent interactions [84].

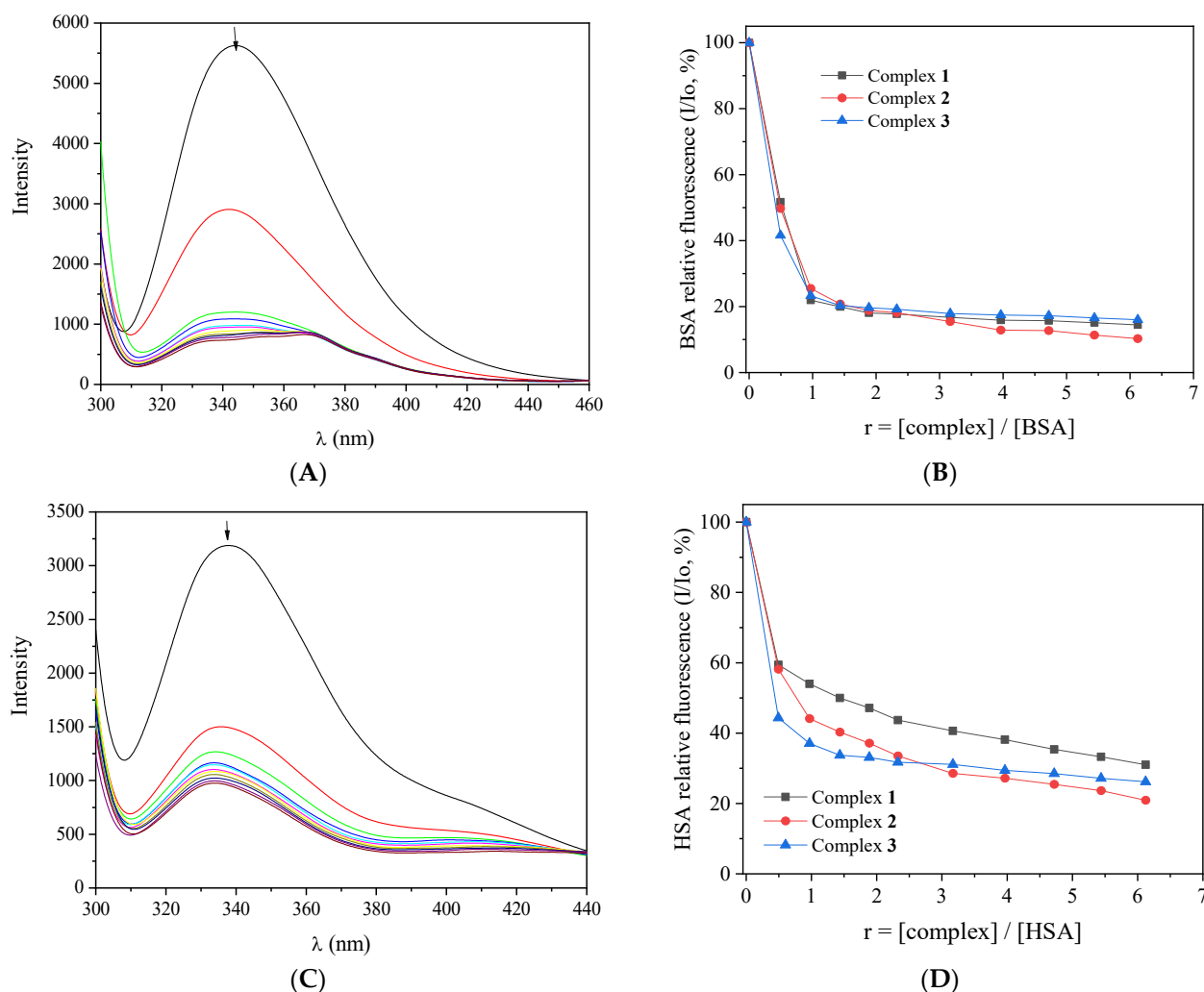


Figure 7. (A) Fluorescence emission spectra ($\lambda_{\text{excitation}} = 295 \text{ nm}$) of BSA ($3 \mu\text{M}$) in buffer solution (150 mM of NaCl and 15 mM of trisodium citrate at pH = 7.0) in the absence and presence of increasing amounts of $[\text{Ni}(3,5\text{-diBr-salo})_2(\text{neoc})]$ (complex 1). (B) Plot of relative BSA-fluorescence emission intensity at $\lambda_{\text{em,max}} = 345 \text{ nm}$ ($I/I_0, \%$) vs. r ($r = [\text{complex}]/[\text{BSA}]$) for complexes 1–3 (up to 14.4% of the initial BSA fluorescence for $[\text{Ni}(3,5\text{-diBr-salo})_2(\text{neoc})]$ (complex 1), 10.3% for $[\text{Ni}(3,5\text{-diBr-salo})_2(\text{phen})]$ (complex 2), and 16.0% for $[\text{Ni}(3,5\text{-diBr-salo})_2(\text{H}_2\text{O})_2]$ (complex 3)). (C) Fluorescence emission spectra ($\lambda_{\text{excitation}} = 295 \text{ nm}$) of HSA ($3 \mu\text{M}$) in buffer solution (150 mM of NaCl and 15 mM of trisodium citrate at pH = 7.0) in the absence and presence of increasing amounts of $[\text{Ni}(3,5\text{-diBr-salo})_2(\text{H}_2\text{O})_2]$ (complex 3). (D) Plot of relative HSA-fluorescence emission intensity at $\lambda_{\text{em,max}} = 340 \text{ nm}$ ($I/I_0, \%$) vs. r ($r = [\text{complex}]/[\text{HSA}]$) for complexes 1–3 (up to 31.0% of the initial HSA fluorescence for $[\text{Ni}(3,5\text{-diBr-salo})_2(\text{neoc})]$ (complex 1), 20.9% for $[\text{Ni}(3,5\text{-diBr-salo})_2(\text{phen})]$ (complex 2), and 26.2% for $[\text{Ni}(3,5\text{-diBr-salo})_2(\text{H}_2\text{O})_2]$ (complex 3)).

3. Materials and Methods

3.1. Materials—Instrumentation—Physical Measurements

All chemicals (3,5-diBr-saloH, phen, neoc, $\text{NiCl}_2 \cdot 6\text{H}_2\text{O}$, CH_3ONa , sodium citrate, NaCl, CT DNA, EB, BSA, and HSA) were used as purchased (reagent grade) from Sigma-Aldrich Co., St. Louis, MI, USA, and all solvents were purchased from ChemLab, Washington, DC, USA. The DNA stock solution was prepared by dilution of CT DNA to a buffer solution (containing 150 mM of NaCl and 15 mM of sodium citrate at pH 7.0) followed by stirring at 4°C , and it was kept at 4°C for no longer than two weeks. The stock solution of CT DNA gave a ratio of UV absorbance at 260 and 280 nm (A_{260}/A_{280}) in the range of 1.85–1.90, indicating that DNA was sufficiently free of protein contamination [85]. The

DNA concentration was determined by the UV absorbance at 260 nm after 1:20 dilution using $\epsilon = 6600 \text{ M}^{-1}\text{cm}^{-1}$ [86].

FT-infrared (FT-IR) spectra were recorded in the range (400–4000 cm^{-1}) on a PerkinElmer (Waltham, MA, USA) FT-IR Spectrum BX spectrometer with samples prepared as KBr pellets (abbreviations used: vs = very strong; s = strong; sm = strong-to-medium; m = medium). The UV–vis spectra were recorded in the range of 200–1100 nm on a dual-beam spectrophotometer Hitachi U–2001 (abbreviation used: sh = shoulder). The spectra were recorded in DMSO solutions using quartz cells with an optical path of 1 cm sealed tightly with Teflon caps. The fluorescence emission spectra were recorded in solution on a Hitachi F–7000 fluorescence spectrophotometer. C, H, and N elemental analyses were performed on a PerkinElmer 240B elemental analyzer. The molar conductivity measurements were carried out on 1 mM of DMSO solution of the complexes with a Crison Basic 30 conductometer. RT magnetic measurements were carried out on a magnetic susceptibility balance of Johnson Matthey Chemicals Limited by the Faraday method (the μ_{eff} values were calculated via the equation: $\mu_{\text{eff}} = 2.83 \sqrt{\chi_{\text{M}}^{\text{corr}} \times T}$, where $\chi_{\text{M}}^{\text{corr}}$ is the corrected magnetic susceptibility of the compound). The viscosity experiments were carried out using an ALPHA L Fungilab rotational viscometer equipped with an 18-mL LCP spindle.

3.2. Synthesis of the Complexes

All complexes were prepared at room temperature according to the following procedure: CH_3ONa (0.5 mmol, 27 mg) was added into a methanolic solution (10 mL) of 3,5-diBr-saloH (0.5 mmol, 70 mg) under stirring for 30 min in order to deprotonate 3,5-dibromo-salicylaldehyde. Afterwards, the resultant solution was added dropwise to a methanolic solution of $\text{NiCl}_2 \cdot 6\text{H}_2\text{O}$ (0.25 mmol, 59 mg). For complexes **1** and **2**, a methanolic solution of the corresponding N,N' -donor (0.25 mmol) was added simultaneously to the reaction solution. The final solution was stirred for additional 45 min and was left to evaporate slowly. The formation of the desired product was observed after a few days.

[Ni(3,5-diBr-salo)₂(neoc)] (complex **1**): For the synthesis of complex **1**, neoc (0.25 mmol, 52 mg) was used as the N,N' -donor. After ten days, green single-crystals of $[\text{Ni}(\text{3,5-Br-salo})_2(\text{neoc})]$ suitable for X-ray structural determination were collected. Yield 80 mg, 40%. *Anal.* calcd. for $\text{C}_{28}\text{H}_{18}\text{NiBr}_4\text{N}_2\text{O}_4$ (MW = 824.79): C 40.77, H 2.20, N 3.40; found: C 40.52, H 2.31, N 3.23%. FT-IR (KBr disk), $\nu_{\text{max}}/\text{cm}^{-1}$: $\nu(\text{C}=\text{O})_{\text{aldehyde}}$, 1641 (s); $\nu(\text{C}-\text{O})_{\text{phenolato}}$, 1340 (sm); $\rho(\text{C}-\text{H})_{\text{neoc}}$, 726 (m). UV–vis: solid, λ/nm : 625, 415; in DMSO, λ/nm ($\epsilon/\text{M}^{-1}\text{cm}^{-1}$): 1025 (sh) (10), 630 (70), 420 (1600), 298 (sh) (5700); $10\text{Dq} = 9756 \text{ cm}^{-1}$, $B = 694 \text{ cm}^{-1}$, $10\text{Dq}/B = 14.0$. Complex **1** is soluble in DMF and DMSO. $\Lambda_{\text{M}} = 12 \text{ S}\cdot\text{cm}^2\cdot\text{mol}^{-1}$, 1 mM in DMSO. μ_{eff} at RT = 2.95 BM.

[Ni(3,5-diBr-salo)₂(phen)] (complex **2**): For the synthesis of complex **2**, phen (0.25 mmol, 45 mg) was used as the N,N' -donor. After a few days, green product of $[\text{Ni}(\text{3,5-Br-salo})_2(\text{phen})]$ (100 mg, 50%) was collected. *Anal.* calcd. for $\text{C}_{26}\text{H}_{14}\text{NiBr}_4\text{N}_2\text{O}_4$ (MW = 796.75): C 39.19, H 1.77, N 3.52; found: C 39.37, H 1.61, N 3.29%. FT-IR (KBr disk), $\nu_{\text{max}}/\text{cm}^{-1}$: $\nu(\text{C}=\text{O})_{\text{aldehyde}}$, 1622 (s); $\nu(\text{C}-\text{O})_{\text{phenolato}}$, 1327 (sm); $\rho(\text{C}-\text{H})_{\text{phen}}$, 732 (m). UV–vis: solid, λ/nm : 645, 425; in DMSO, λ/nm ($\epsilon/\text{M}^{-1}\text{cm}^{-1}$): 1025 (sh) (5), 665 (50), 422 (1300), 296 (sh) (5800); $10\text{Dq} = 9756 \text{ cm}^{-1}$, $B = 631 \text{ cm}^{-1}$, $10\text{Dq}/B = 15.5$. Complex **2** is soluble in DMF and DMSO. $\Lambda_{\text{M}} = 15 \text{ S}\cdot\text{cm}^2\cdot\text{mol}^{-1}$, 1 mM in DMSO. μ_{eff} at RT = 2.98 BM.

[Ni(3,5-diBr-salo)₂(CH₃OH)₂] (complex **3**): Complex **3** was prepared in the absence of a N,N' -donor. After a few days, light-green product of $[\text{Ni}(\text{3,5-Br-salo})_2(\text{MeOH})_2]$, (95 mg, 55%) was collected by filtration. *Anal.* calcd. for $\text{C}_{16}\text{H}_{14}\text{Br}_4\text{NiO}_6$ (MW = 680.63): C 28.23, H 2.07; found: C 27.95, H 2.25%. FT-IR (KBr disk), $\nu_{\text{max}}/\text{cm}^{-1}$: $\nu(\text{C}=\text{O})_{\text{aldehyde}}$, 1647 (vs); $\nu(\text{C}-\text{O})_{\text{phenolato}}$, 1315 (s). UV–vis: solid, λ/nm : 655, 415; in DMSO, λ/nm ($\epsilon/\text{M}^{-1}\text{cm}^{-1}$): 1040 (sh) (5), 670 (25), 421 (1260), 302 (sh) (6500); $10\text{Dq} = 9615 \text{ cm}^{-1}$, $B = 655 \text{ cm}^{-1}$, $10\text{Dq}/B = 14.7$. Complex **3** is soluble in DMSO, DMF, and MeOH. $\Lambda_{\text{M}} = 10 \text{ S}\cdot\text{cm}^2\cdot\text{mol}^{-1}$, 1 mM in DMSO. μ_{eff} at RT = 3.00 BM.

3.3. Single-Crystal X-ray Crystallography

A crystal of complex **1** suitable for X-ray structural determination was mounted at RT on a Bruker Kappa APEX2 diffractometer equipped with a Triumph monochromator using Mo K α ($\lambda = 0.71073 \text{ \AA}$, source operating at 50 kV and 30 mA) radiation. Unit cell dimensions were determined and refined by using the angular settings of at least 168 high-intensity reflections ($>10\sigma(I)$) in the range $10^\circ < 2\theta < 20^\circ$. Intensity data were recorded using φ and ω scans. All crystals presented no decay during the data collection. The frames collected for each crystal were integrated with the Bruker SAINT Software package (Version 2) using a narrow-frame algorithm [87]. Data were corrected for absorption using the numerical method (SADABS) based on crystal dimensions [88]. All structures were solved using SUPERFLIP [89] incorporated in Crystals. Data refinement (full-matrix least-squares methods on F^2) and all subsequent calculations were conducted using the Crystals version 14.61 build 6720 program package [90]. All non-hydrogen non-disordered atoms were refined anisotropically. Hydrogen atoms were located from difference Fourier maps and refined at idealized positions riding on the parent atoms with isotropic displacement parameters $U_{\text{iso}}(\text{H}) = 1.2U_{\text{eq}}(\text{C})$ at distances C–H 0.95 \AA .

Crystallographic data for complex **1** are presented in Table 1. Further details on the crystallographic studies as well as atomic displacement parameters are given as Supporting Information in the form of cif files. CCDC deposition number 2346279 contains the supplementary crystallographic data for this paper. These data can be obtained free of charge via www.ccdc.cam.ac.uk/conts/retrieving.html (or from the Cambridge Crystallographic Data Centre, 12 Union Road, Cambridge CB21EZ, UK; fax: (+44) 1223–336–033; or deposit@ccdc.cam.ac.uk).

3.4. Study of the Biological Profile of the Complexes

The *in vitro* evaluation of the biological activity of the complexes, i.e., interaction with CT DNA and albumins, was conducted following the dissolution of the complexes in DMSO (1 mM) due to their limited solubility in water. The experiments were carried out in the presence of aqueous buffer solutions, ensuring that the ratio of DMSO in the final solution did not exceed 5% (*v/v*). Control experiments were implemented to evaluate the impact of DMSO on the data. Minimal-to-no alterations were observed in the spectra of albumins or CT DNA, and appropriate adjustments were made as necessary. The interaction of the compounds with CT DNA was examined thoroughly by DNA-viscosity measurements, UV–vis spectroscopy titrations, and through competitive studies with EB by fluorescence emission spectroscopy. The albumin-binding was studied through tryptophan fluorescence quenching experiments. All the experimental protocols and the equations employed for these studies are described in the Supplementary File (Sections S1 and S2).

4. Conclusions

Three nickel(II) complexes with 3,5-dibromo-salicylaldehyde (3,5-diBr-saloH) were synthesized, in the presence or absence of two phenanthroline derivatives, i.e., 1,10-phenanthroline (phen) and 2,9-dimethyl-1,10-phenanthroline (neoc). The 3,5-diBr-salo[−] ligands are bound to the nickel(II) ion bidentately through the deprotonated phenolato and the carbonyl oxygen atoms. The nickel(II) ions are six-coordinated with a distorted octahedral geometry.

The complexes interact with linear calf-thymus DNA via intercalation and bind tightly and reversibly to human and serum albumins, as revealed by the corresponding binding constants determined. The presence of a *N,N'*-donor co-ligand (neoc in complex **1** and phen in complex **2**) resulted in higher DNA-binding constants when compared with complex **3** (absence of *N,N'*-donor co-ligand), while the opposite tendency was found for the albumin-binding constants where complex **3** presented the highest constants.

In total, complexes **1–3** showed promising features regarding the interaction with biomolecules, thus constituting the trigger for further bioactivity studies in future projects.

Supplementary Materials: The following supporting information can be downloaded at: <https://www.mdpi.com/article/10.3390/inorganics12050138/s1>, Cif file for compound 1; checkcif file for compound 1; Supplementary file containing: S1. Protocols for interaction studies with CT DNA; S2. Protocols for interaction studies with serum albumins; Figure S1: IR spectra of complexes 1–3; Figure S2: UV-vis spectra of complexes 1–3 in DMSO solution; Figure S3. UV-vis spectra of complexes 1–3 in solid state; Figure S4: Plot of $[DNA]/(\epsilon_A - \epsilon_F)$ vs. $[DNA]$ for complexes 1–3; Figure S5: Stern–Volmer quenching plot of EB–DNA fluorescence for complexes 1–3; Figure S6: Stern–Volmer quenching plot of BSA fluorescence for complexes 1–3; Figure S7: Stern–Volmer quenching plot of HSA fluorescence for complexes 1–3; Figure S8: Scatchard plot of BSA of complexes 1–3; Figure S9: Scatchard plot of HSA of complexes 1–3 [72,76,77,81,82].

Author Contributions: Conceptualization, G.I.P., A.Z. and G.P.; methodology, G.I.P., A.Z. and G.P.; formal analysis, G.I.P., A.Z., A.G.H. and G.P.; investigation, G.I.P., A.Z. and A.G.H.; resources, A.G.H. and G.P.; data curation, G.I.P., A.Z., A.G.H. and G.P.; writing—original draft preparation, G.I.P., A.Z., A.G.H. and G.P.; writing—review and editing, G.P.; supervision, G.P.; project administration, G.P.; funding acquisition, G.P. All authors have read and agreed to the published version of the manuscript.

Funding: This research received no external funding.

Data Availability Statement: Data are contained within the article and Supplementary Materials.

Conflicts of Interest: The authors declare no conflicts of interest.

Abbreviations

3,5-diBr-saloH = 3,5-dibromo-salicylaldehyde; 3,5-diCl-saloH = 3,5-dichloro-salicylaldehyde; 5-Br-saloH = 5-bromo-salicylaldehyde; 5-Cl-saloH = 5-chloro-salicylaldehyde; 5-NO₂-saloH = 5-nitro-salicylaldehyde; bipy = 2,2'-bipyridine; bipyam = 2,2'-bipyridylamine; BSA = bovine serum albumin; CT = calf thymus; EB = ethidium bromide, 3,8-diamino-5-ethyl-6-phenyl-phenanthridinium bromide; HSA = human serum albumin; K = SA-binding constant; K_b = DNA-binding constant; K_q = quenching constant; K_{SV} = Stern–Volmer constant; neoc = 2,9-dimethyl-1,10-phenanthroline, neocuproine; phen = 1,10-phenanthroline; r = [compound]/[DNA] ratio or [compound]/[albumin] ratio; RT = room -temperature; SA = serum albumin; saloH = salicylaldehyde; X-saloH = substituted salicylaldehyde.

References

1. Claudel, M.; Schwarte, J.V.; Fromm, K.M. New Antimicrobial Strategies Based on Metal Complexes. *Chemistry* **2020**, *2*, 849–899. [CrossRef]
2. Gasser, G. Metal Complexes and Medicine: A Successful Combination. *Chimia* **2015**, *69*, 442–446. [CrossRef] [PubMed]
3. Pauls, G.; Becker, T.; Rahfeld, P.; Gretscher, R.R.; Paetz, C.; Pasteels, J.; von Reuss, S.H.; Burse, A.; Boland, W. Two Defensive Lines in Juvenile Leaf Beetles; Esters of 3-Nitropropionic Acid in the Hemolymph and Aposematic Warning. *J. Chem. Ecol.* **2016**, *42*, 240–248. [CrossRef] [PubMed]
4. Kumar, S.; Devi, J.; Dubey, A.; Kumar, D.; Jindal, D.K.; Asija, S.; Sharma, A. Co(II), Ni(II), Cu(II) and Zn(II) Complexes of Schiff Base Ligands: Synthesis, Characterization, DFT, in Vitro Antimicrobial Activity and Molecular Docking Studies. *Res. Chem. Intermed.* **2023**, *49*, 939–965. [CrossRef]
5. Kargar, H.; Ardakani, A.A.; Tahir, M.N.; Ashfaq, M.; Munawar, K.S. Synthesis, Spectral Characterization, Crystal Structure Determination and Antimicrobial Activity of Ni(II), Cu(II) and Zn(II) Complexes with the Schiff Base Ligand Derived from 3,5-Dibromosalicylaldehyde. *J. Mol. Struct.* **2021**, *1229*, 129842. [CrossRef]
6. Ghasemi, L.; Abedi, A.; Abbasi, A.; Kucerakova, M.; Dusek, M.; Behzad, M. Subtle Structural Variations in New Mixed-Ligand Cu(II) Complexes with NN'O Type Unsymmetrical Schiff Bases: Molecular Docking against SARS-CoV-2 and Its Omicron Variant Main Proteases. *Inorg. Chem. Commun.* **2024**, *159*, 111795. [CrossRef]
7. Zianna, A.; Geromichalos, G.D.; Pekou, A.; Hatzidimitriou, A.G.; Coutouli-Argyropoulou, E.; Lalia-Kantouri, M.; Pantazaki, A.A.; Psomas, G. A Palladium(II) Complex with the Schiff Base 4-Chloro-2-(N-Ethyliminomethyl)-Phenol: Synthesis, Structural Characterization, and in Vitro and in Silico Biological Activity Studies. *J. Inorg. Biochem.* **2019**, *199*, 110792. [CrossRef] [PubMed]
8. Kargar, H.; Centore, R.; Fallah-Mehrjardi, M.; Santagata, E.; Munawar, K.S. Dihalosalicylaldehyde Based Molybdenum(VI) Complexes: Synthesis, Spectral Characterization, Crystal Structures, and Catalytic Activities for the Selective Oxidation of Benzylic Alcohols. *Inorg. Chim. Acta* **2024**, *566*, 122015. [CrossRef]

9. Karmakar, M.; Kumar, P.; Jiyaur Rahaman, S.; Chattopadhyay, S. An Overview on the Synthesis, Structure, and Application of Vanadyl Complexes with Hydrazonic Acid Ligands Based on Salicylaldehyde or Its Derivatives. *Inorg. Chim. Acta* **2024**, *565*, 121969. [[CrossRef](#)]
10. Zhuo, S.; Wu, W.; Liu, Y.; Zou, L.; Wu, Y.; Botha, L.; Kumar, A.; Afzal, M.; Alarifi, A. 3,5-Dibromosalicylaldehyde Nicotinoylhydrazone and 4,4'-Bipyridine Appended New Zn(II) Coordination Polymer: Secnidazole Sensing and Rhodamine B Photocatalytic Degradation Properties. *J. Mol. Struct.* **2022**, *1264*, 133304. [[CrossRef](#)]
11. Gui, M.; Wu, W.; Liu, Y.; Wu, Y.; Singh, S.; Kumar, A.; Afzal, M.; Alarifi, A.; Shi, C. Sensing and Photocatalytic Properties of a New 1D Zn(II)-Based Coordination Polymer Derived from the 3,5-Dibromosalicylaldehyde Nicotinoylhydrazone Ligand. *Polyhedron* **2022**, *222*, 115900. [[CrossRef](#)]
12. Rani, M.; Devi, J.; Kumar, B.; Arora, T.; Taxak, B. Tridentate Xanthene-Based Hydrazone Ligands and Their Mononuclear Transition Metal Complexes: Synthesis, Anti-Malarial, Antimicrobial and Molecular Docking Studies. *Res. Chem. Intermed.* **2024**, *50*, 1409–1434. [[CrossRef](#)]
13. Zahirović, A.; Hadžalić, S.; Višnjevac, A.; Fočak, M.; Tüzün, B.; Žilić, D.; Roca, S.; Jurec, J.; Topčagić, A.; Osmanković, I. Vanadium(IV) Complexes of Salicylaldehyde-Based Furoic Acid Hydrazones: Synthesis, BSA Binding and in Vivo Antidiabetic Potential. *J. Inorg. Biochem.* **2023**, *244*, 112232. [[CrossRef](#)]
14. Adhikari, H.S.; Garai, A.; Khanal, C.; Yadav, P.N. Synthesis and Comprehensive Characterization with Anticancer Activity Assessment of Salicylaldehyde and 2-Acetylphenol Based Chitosan Thiosemicarbazones and Their Copper(II) Complexes. *Carbohydr. Polym. Technol. Appl.* **2024**, *7*, 100469. [[CrossRef](#)]
15. Scaccaglia, M.; Pinelli, S.; Manini, L.; Ghezzi, B.; Nicastro, M.; Heinrich, J.; Kulak, N.; Mozzoni, P.; Pelosi, G.; Bisceglie, F. Gold(III) Complexes with Thiosemicarbazone Ligands: Insights into Their Cytotoxic Effects on Lung Cancer Cells. *J. Inorg. Biochem.* **2024**, *251*, 112438. [[CrossRef](#)]
16. Andriichuk, Y.M.; Lyapunov, A.Y.; Hotynchan, A.H.; Savchenko, D.V.; Karavan, V.V.; Turash, M.M.; Khalavka, Y.B. Synergetic Radical-Scavenging Effect in the Complex of Copper(II) with the Thiosemicarbazone of Salicylaldehyde. *J. Coord. Chem.* **2023**, *76*, 1763–1775. [[CrossRef](#)]
17. Elo, H.; Kuure, M.; Peltari, E. Correlation of the Antimicrobial Activity of Salicylaldehydes with Broadening of the NMR Signal of the Hydroxyl Proton. Possible Involvement of Proton Exchange Processes in the Antimicrobial Activity. *Eur. J. Med. Chem.* **2015**, *92*, 750–753. [[CrossRef](#)] [[PubMed](#)]
18. Peltari, E.; Lehtinen, M.; Elo, H. Substituted Salicylaldehydes as Potential Antimicrobial Drugs: Minimal Inhibitory and Microbicidal Concentrations. *Z. Naturforsch.—Sect. C J. Biosci.* **2011**, *66*, 571–580. [[CrossRef](#)]
19. Kordestani, N.; Rudbari, H.A.; Fernandes, A.R.; Raposo, L.R.; Baptista, P.V.; Ferreira, D.; Bruno, G.; Bella, G.; Scopelliti, R.; Braun, J.D.; et al. Antiproliferative Activities of Diimine-Based Mixed Ligand Copper(II) Complexes. *ACS Comb. Sci.* **2020**, *22*, 89–99. [[CrossRef](#)] [[PubMed](#)]
20. Varadwaj, P.R.; Varadwaj, A.; Marques, H.M. Halogen Bonding: A Halogen-Centered Noncovalent Interaction Yet to Be Understood. *Inorganics* **2019**, *7*, 40. [[CrossRef](#)]
21. Feng, D.; Wang, B.; Wang, L.; Abraham, N.; Tao, K.; Huang, L.; Shi, W.; Dong, Y.; Qu, Y. Pre-Ischemia Melatonin Treatment Alleviated Acute Neuronal Injury after Ischemic Stroke by Inhibiting Endoplasmic Reticulum Stress-Dependent Autophagy via PERK and IRE1 Signalings. *J. Pineal Res.* **2017**, *62*, e12395. [[CrossRef](#)]
22. Thapa, K.; Khan, H.; Singh, T.G.; Kaur, A. Traumatic Brain Injury: Mechanistic Insight on Pathophysiology and Potential Therapeutic Targets. *J. Mol. Neurosci.* **2021**, *71*, 1725–1742. [[CrossRef](#)] [[PubMed](#)]
23. Vitomirov, T.; Dimiza, F.; Matić, I.Z.; Stanojković, T.; Pirković, A.; Živković, L.; Spremo-Potparević, B.; Novaković, I.; Anđelković, K.; Milčić, M.; et al. Copper(II) Complexes with 4-(Diethylamino)Salicylaldehyde and α -Diimines: Anticancer, Antioxidant, Antigenotoxic Effects and Interaction with DNA and Albumins. *J. Inorg. Biochem.* **2022**, *235*, 111942. [[CrossRef](#)]
24. Ntanatsidis, S.; Perontsis, S.; Konstantopoulou, S.; Kalogiannis, S.; Hatzidimitriou, A.G.; Papadopoulos, A.N.; Psomas, G. Manganese(II) Complexes of Substituted Salicylaldehydes and α -Diimines: Synthesis, Characterization and Biological Activity. *J. Inorg. Biochem.* **2022**, *227*, 111693. [[CrossRef](#)]
25. Papadopoulos, Z.; Doulopoulou, E.; Zianna, A.; Hatzidimitriou, A.G.; Psomas, G. Copper(II) Complexes of 5-Fluoro-Salicylaldehyde: Synthesis, Characterization, Antioxidant Properties, Interaction with DNA and Serum Albumins. *Molecules* **2022**, *27*, 8929. [[CrossRef](#)]
26. Zianna, A.; Vradi, E.; Hatzidimitriou, A.G.; Kalogiannis, S.; Psomas, G. Zinc(II) Complexes of 3-Bromo-5-Chloro-Salicylaldehyde: Characterization and Biological Activity. *Dalton Trans.* **2022**, *51*, 17629–17641. [[CrossRef](#)]
27. Zianna, A.; Geromichalos, G.; Psoma, E.; Kalogiannis, S.; Hatzidimitriou, A.G.; Psomas, G. Structure and in Vitro and in Silico Biological Activity of Zinc(II) Complexes with 3,5-Dichloro-Salicylaldehyde. *J. Inorg. Biochem.* **2022**, *229*, 111727. [[CrossRef](#)]
28. Zianna, A.; Geromichalou, E.; Geromichalos, G.; Fiotaki, A.M.; Hatzidimitriou, A.G.; Kalogiannis, S.; Psomas, G. Zinc(II) Complexes of 3,5-Dibromo-Salicylaldehyde and α -Diimines: Synthesis, Characterization and in Vitro and in Silico Biological Profile. *J. Inorg. Biochem.* **2022**, *226*, 111659. [[CrossRef](#)]
29. Christidou, A.; Zavalani, K.; Hatzidimitriou, A.G.; Psomas, G. Copper(II) Complexes with 3,5-Dihalogeno-Salicylaldehydes: Synthesis, Structure and Interaction with DNA and Albumins. *J. Inorg. Biochem.* **2023**, *238*, 112049. [[CrossRef](#)] [[PubMed](#)]
30. Aryaeifar, M.; Rudbari, H.A.; Moreno-Pineda, E.; Cuevas-Vicario, J.V.; Paul, S.; Schulze, M.; Wernsdorfer, W.; Lloret, F.; Moini, N.; Blacque, O. Synthesis, Characterization and Magnetic Properties of Halogenated Tetranuclear Cubane-like Nickel(II) Complexes. *New J. Chem.* **2024**, *48*, 3603–3613. [[CrossRef](#)]

31. Zianna, A.; Geromichalos, G.; Fiotaki, A.M.; Hatzidimitriou, A.G.; Kalogiannis, S.; Psomas, G. Palladium(II) Complexes of Substituted Salicylaldehydes: Synthesis, Characterization and Investigation of Their Biological Profile. *Pharmaceuticals* **2022**, *15*, 886. [[CrossRef](#)]
32. Fontecilla-Camps, J.C. Nickel and the Origin and Early Evolution of Life. *Metallomics* **2022**, *14*, 16. [[CrossRef](#)]
33. Meyer, F.; Kozłowski, H. Nickel. *Compr. Coord. Chem. II* **2004**, *6*, 247–554. [[CrossRef](#)]
34. Kumar, S.; Trivedi, A.V. A Review on Role of Nickel in the Biological System. *Int. J. Curr. Microbiol. Appl. Sci.* **2016**, *5*, 719–727. [[CrossRef](#)]
35. Prueitt, R.L.; Li, W.; Chang, Y.C.; Boffetta, P.; Goodman, J.E. Systematic Review of the Potential Respiratory Carcinogenicity of Metallic Nickel in Humans. *Crit. Rev. Toxicol.* **2020**, *50*, 605–639. [[CrossRef](#)]
36. Buttice, C. Nickel. In *The SAGE Encyclopedia of Cancer and Society*; Colditz, G.A., Ed.; SAGE Publications: Thousand Oaks, CA, USA, 2015; Volume 2, pp. 828–831.
37. Zhao, J.; Shi, X.; Castranova, V.; Ding, M. Occupational Toxicology of Nickel and Nickel Compounds. *J. Environ. Pathol. Toxicol. Oncol.* **2009**, *28*, 177–208. [[CrossRef](#)]
38. Barceloux, D.G. Nickel. *J. Toxicol. Clin. Toxicol.* **1999**, *37*, 239–258. [[CrossRef](#)]
39. Dixon, N.E.; Gazzola, C.; Blakeley, R.L.; Zerner, B. Jack Bean Urease (EC 3.5.1.5). A Metalloenzyme. A Simple Biological Role for Nickel? *J. Am. Chem. Soc.* **1975**, *97*, 4131–4133. [[CrossRef](#)]
40. Company, A.; McDonald, A.R. Bio-Relevant Chemistry of Nickel. In *Comprehensive Coordination Chemistry III*; Constable Edwin, C., Parkin, G., Que, L., Jr., Eds.; Elsevier: Hoboken, NJ, USA, 2021; Volume 8, pp. 846–877, ISBN 9780081026885.
41. Glazer, E.C.; Casini, A. Metals in Medicine. *Eur. J. Inorg. Chem.* **2022**, *2022*, e202101093. [[CrossRef](#)]
42. Orvig, C.; Abrams, M.J. Medicinal Inorganic Chemistry: Introduction. *Chem. Rev.* **1999**, *99*, 2202–2203. [[CrossRef](#)]
43. Bisceglie, F.; Pinelli, S.; Alinovi, R.; Goldoni, M.; Mutti, A.; Camerini, A.; Piola, L.; Tarasconi, P.; Pelosi, G. Cinnamaldehyde and Cuminlaldehyde Thiosemicarbazones and Their Copper(II) and Nickel(II) Complexes: A Study to Understand Their Biological Activity. *J. Inorg. Biochem.* **2014**, *140*, 111–125. [[CrossRef](#)] [[PubMed](#)]
44. Betanzos-Lara, S.; Gómez-Ruiz, C.; Barrón-Sosa, L.R.; Gracia-Mora, I.; Flores-Álamo, M.; Barba-Behrens, N. Cytotoxic Copper(II), Cobalt(II), Zinc(II), and Nickel(II) Coordination Compounds of Clotrimazole. *J. Inorg. Biochem.* **2012**, *114*, 82–93. [[CrossRef](#)] [[PubMed](#)]
45. Haribabu, J.; Jeyalakshmi, K.; Arun, Y.; Bhuvanesh, N.S.P.; Perumal, P.T.; Karvembu, R. Synthesis, DNA/Protein Binding, Molecular Docking, DNA Cleavage and in Vitro Anticancer Activity of Nickel(II) Bis(Thiosemicarbazone) Complexes. *RSC Adv.* **2015**, *5*, 46031–46049. [[CrossRef](#)]
46. Kisa, D.; Korkmaz, N.; Taslimi, P.; Tuzun, B.; Tekin, Ş.; Karadag, A.; Sen, F. Bioactivity and Molecular Docking Studies of Some Nickel Complexes: New Analogues for the Treatment of Alzheimer, Glaucoma and Epileptic Diseases. *Bioorg Chem.* **2020**, *101*, 104066. [[CrossRef](#)] [[PubMed](#)]
47. Alomar, K.; Landreau, A.; Allain, M.; Bouet, G.; Larcher, G. Synthesis, Structure and Antifungal Activity of Thiophene-2,3-Dicarboxaldehyde Bis(Thiosemicarbazone) and Nickel(II), Copper(II) and Cadmium(II) Complexes: Unsymmetrical Coordination Mode of Nickel Complex. *J. Inorg. Biochem.* **2013**, *126*, 76–83. [[CrossRef](#)] [[PubMed](#)]
48. Shawish, H.B.; Wong, W.Y.; Wong, Y.L.; Loh, S.W.; Looi, C.Y.; Hassandarvish, P.; Phan, A.Y.L.; Wong, W.F.; Wang, H.; Paterson, I.C.; et al. Nickel(II) Complex of Polyhydroxybenzaldehyde N4-Thiosemicarbazone Exhibits Anti-Inflammatory Activity by Inhibiting NF-KB Transactivation. *PLoS ONE* **2014**, *9*, e100933. [[CrossRef](#)] [[PubMed](#)]
49. Skyrianou, K.C.; Efthimiadou, E.K.; Psycharis, V.; Terzis, A.; Kessissoglou, D.P.; Psomas, G. Nickel-Quinolones Interaction. Part 1—Nickel(II) Complexes with the Antibacterial Drug Sparfloxacin: Structure and Biological Properties. *J. Inorg. Biochem.* **2009**, *103*, 1617–1625. [[CrossRef](#)]
50. Xu, B.B.; Pei, X.S.; Guan, Q.Y.; Shi, X.; Zhao, G.L. Synthesis, Crystal Structure, and Biological Activity of a Nickel(II) Complex Constructed by 2-Phenyl-4-Selenazole Carboxylic Acid and 1,10-Phenanthroline. *J. Coord. Chem.* **2013**, *66*, 2605–2614. [[CrossRef](#)]
51. Totta, X.; Papadopoulou, A.A.; Hatzidimitriou, A.G.; Papadopoulos, A.; Psomas, G. Synthesis, Structure and Biological Activity of Nickel(II) Complexes with Mefenamato and Nitrogen-Donor Ligands. *J. Inorg. Biochem.* **2015**, *145*, 79–93. [[CrossRef](#)]
52. Perontsis, S.; Hatzidimitriou, A.G.; Papadopoulos, A.N.; Psomas, G. Nickel-Difluoride Complexes: Synthesis, Characterization, in Vitro Antioxidant Activity and Interaction with DNA and Albumins. *J. Inorg. Biochem.* **2016**, *162*, 9–21. [[CrossRef](#)]
53. Lazou, M.; Hatzidimitriou, A.G.; Papadopoulos, A.N.; Psomas, G. Transition Metal(II) Complexes with the Non-Steroidal Anti-Inflammatory Drug Oxaprozin: Characterization and Biological Profile. *J. Inorg. Biochem.* **2023**, *243*, 112196. [[CrossRef](#)]
54. Barmpa, A.; Geromichalos, G.D.; Hatzidimitriou, A.G.; Psomas, G. Nickel(II)–Meclofenamate Complexes: Structure, in Vitro and in Silico DNA– and Albumin–Binding Studies, Antioxidant and Anticholinergic Activity. *J. Inorg. Biochem.* **2021**, *222*, 111507. [[CrossRef](#)] [[PubMed](#)]
55. Zianna, A.; Psomas, G.; Hatzidimitriou, A.; Lalia-Kantouri, M. Ni(II) Complexes with 2,2-Dipyridylamine and Salicylaldehydes: Synthesis, Crystal Structure and Interaction with Calf-Thymus DNA and Albumins. *J. Inorg. Biochem.* **2016**, *163*, 131–142. [[CrossRef](#)]
56. Zianna, A.; Psomas, G.; Hatzidimitriou, A.; Lalia-Kantouri, M. Synthesis, Structural, Thermal Characterization and Interaction with Calf-Thymus DNA and Albumins of Cationic Ni(II) Complexes with 2,2'-Dipyridylamine and Salicylaldehydes. *Polyhedron* **2017**, *124*, 104–116. [[CrossRef](#)]
57. Gkritzali, M.; Georgila, M.; Hatzidimitriou, A.G.; Kalogiannis, S.; Psomas, G. Neutral and Cationic Nickel(II) Complexes with Substituted Salicylaldehydes: Characterization, Antibacterial Activity, and Interaction with Biomacromolecules. *J. Inorg. Biochem.* **2023**, *247*, 112339. [[CrossRef](#)] [[PubMed](#)]

58. Geary, W.J. The Use of Conductivity Measurements in Organic Solvents for the Characterisation of Coordination Compounds. *Coord. Chem. Rev.* **1971**, *7*, 81–122. [[CrossRef](#)]
59. Nakamoto, K. *Infrared and Raman Spectra of Inorganic and Coordination Compounds: Part B: Applications in Coordination, Organometallic, and Bioinorganic Chemistry*; John Wiley and Sons: Hoboken, NJ, USA, 2008; ISBN 9780471744931.
60. Totta, X.; Hatzidimitriou, A.G.; Papadopoulos, A.N.; Psomas, G. Nickel(II)-Naproxen Mixed-Ligand Complexes: Synthesis, Structure, Antioxidant Activity and Interaction with Albumins and Calf-Thymus DNA. *New J. Chem.* **2017**, *41*, 4478–4492. [[CrossRef](#)]
61. Stamou, P.; Hatzidimitriou, A.G.; Psomas, G. Manganese(II) Complexes with 5-Nitro-2-Hydroxy-Benzaldehyde or Substituted 2-Hydroxy-Phenones: Structure and Interaction with Bovine Serum Albumin and Calf-Thymus DNA. *J. Inorg. Biochem.* **2022**, *235*, 111923. [[CrossRef](#)] [[PubMed](#)]
62. Zianna, A.; Psomas, G.; Hatzidimitriou, A.; Coutouli-Argyropoulou, E.; Lalia-Kantouri, M. Zinc Complexes of Salicylaldehydes: Synthesis, Characterization and DNA-Binding Properties. *J. Inorg. Biochem.* **2013**, *127*, 116–126. [[CrossRef](#)]
63. Zianna, A.; Ristović, M.Š.; Psomas, G.; Hatzidimitriou, A.; Coutouli-Argyropoulou, E.; Lalia-Kantouri, M. Cadmium(II) Complexes of 5-Bromo-Salicylaldehyde and α -Diimines: Synthesis, Structure and Interaction with Calf-Thymus DNA and Albumins. *Polyhedron* **2016**, *107*, 136–147. [[CrossRef](#)]
64. Zianna, A.; Sumar Ristic, M.; Psomas, G.; Hatzidimitriou, A.; Coutouli-Argyropoulou, E.; Lalia-Kantouri, M. Cadmium(II) Complexes of 5-Nitro-Salicylaldehyde and α -Diimines: Synthesis, Structure and Interaction with Calf-Thymus DNA. *J. Coord. Chem.* **2015**, *68*, 4444–4463. [[CrossRef](#)]
65. Papadopoulos, C.D.; Lalia-Kantouri, M.; Jaud, J.; Hatzidimitriou, A.G. Substitution Effect on New Co(II) Addition Compounds with Salicylaldehydes and the Nitrogenous Bases Phen or Neoc: Crystal and Molecular Structures of $[\text{Co}^{\text{II}}(5\text{-NO}_2\text{-Salicylaldehyde})_2(\text{Phen})]$, $[\text{Co}^{\text{II}}(5\text{-CH}_3\text{-Salicylaldehyde})_2(\text{Neoc})]$ and $[\text{Co}^{\text{II}}(5\text{-Cl-Salicylaldehyde})_2(\text{Neoc})]$. *Inorg. Chim. Acta* **2007**, *360*, 3581–3589. [[CrossRef](#)]
66. Papadopoulos, C.D.; Hatzidimitriou, A.G.; Voutsas, G.P.; Lalia-Kantouri, M. Synthesis and Characterization of New Addition Compounds of Bis(Substituted-Salicylaldehyde)Cobalt(II) with 2,2'-Bipyridine (Bipy). Crystal and Molecular Structures of $[\text{Co}^{\text{II}}(3\text{-Methoxy-Salicylaldehyde})_2(\text{Bipy})]\cdot\text{CH}_3\text{OH}$ (1) and $[\text{Co}^{\text{II}}(\text{Bipy})_3]\text{Br}_2\cdot 0.5(5\text{-Chloro-SalicylaldehydeH})\cdot 1.5\text{CH}_3\text{OH}$ (5). *Polyhedron* **2007**, *26*, 1077–1086. [[CrossRef](#)]
67. Lalia-Kantouri, M.; Gdaniec, M.; Czapik, A.; Chrissafis, K.; Ferenc, W.; Sarzynski, J.; Papadopoulos, C.D. Thermoanalytical, Magnetic and Structural Study of Co(II) Complexes with Substituted Salicylaldehydes and Neocuproine. *J. Therm. Anal. Calorim.* **2012**, *109*, 131–139. [[CrossRef](#)]
68. Papadopoulos, C.; Cristóvão, B.; Ferenc, W.; Hatzidimitriou, A.; Cipriotti, S.V.; Risoluti, R.; Lalia-Kantouri, M. Thermoanalytical, Magnetic and Structural Investigation of Neutral Co(II) Complexes with 2,2'-Dipyridylamine and Salicylaldehydes. *J. Therm. Anal. Calorim.* **2016**, *123*, 717–729. [[CrossRef](#)]
69. Pages, B.J.; Ang, D.L.; Wright, E.P.; Aldrich-Wright, J.R. Metal Complex Interactions with DNA. *Dalton Trans.* **2015**, *44*, 3505–3526. [[CrossRef](#)] [[PubMed](#)]
70. Duchackova, L.; Steinmetz, V.; Lemaire, J.; Roithova, J. Comparison of 2,2'-Bipyridine and 2,2'-Bipyridyl-N,N'-Dioxide as Ligands in Zinc Complexes. *Inorg. Chem.* **2010**, *49*, 8897–8903. [[CrossRef](#)] [[PubMed](#)]
71. Wilson, W.D.; Paul, A. Reversible Small Molecule–Nucleic Acid Interactions. In *Nucleic Acids in Chemistry and Biology*; Blackburn, G.M., Egli, M., Gait, M.J., Watts, J.K., Eds.; The Royal Society of Chemistry: London, UK, 2022; pp. 477–521.
72. Wolfe, A.; Shimer, G.H.; Meehan, T. Polycyclic Aromatic Hydrocarbons Physically Intercalate into Duplex Regions of Denatured DNA. *Biochemistry* **1987**, *26*, 6392–6396. [[CrossRef](#)] [[PubMed](#)]
73. Dimitrakopoulou, A.; Dendrinou-Samara, C.; Pantazaki, A.A.; Alexiou, M.; Nordlander, E.; Kessissoglou, D.P. Synthesis, Structure and Interactions with DNA of Novel Tetranuclear, $[\text{Mn}_4(\text{II}/\text{II}/\text{II}/\text{IV})]$ Mixed Valence Complexes. *J. Inorg. Biochem.* **2008**, *102*, 618–628. [[CrossRef](#)]
74. Gkisiou, C.; Malis, G.; Hatzidimitriou, A.G.; Psomas, G. Erbium(III) Coordination Compounds with Substituted Salicylaldehydes: Characterization and Biological Profile. *J. Inorg. Biochem.* **2023**, *242*, 112161. [[CrossRef](#)]
75. Garcia-Gimenez, J.L.; Gonzalez-Alvarez, M.; Liu-Gonzalez, M.; Macías, B.; Borrás, J.; Alzuet, G. Toward the Development of Metal-Based Synthetic Nucleases: DNA Binding and Oxidative DNA Cleavage of a Mixed Copper(II) Complex with N-(9H-Purin-6-yl)Benzenesulfonamide and 1,10-Phenanthroline. Antitumor Activity in Human Caco-2 Cells and Jurkat T Lymphocytes. Evaluation of P53 and Bcl-2 Proteins in the Apoptotic Mechanism. *J. Inorg. Biochem.* **2009**, *103*, 923–934. [[CrossRef](#)] [[PubMed](#)]
76. Lakowicz, J.R. *Principles of Fluorescence Spectroscopy*; Springer: Berlin/Heidelberg, Germany, 2006; ISBN 0387312781.
77. Heller, D.P.; Greenstock, C.L. Fluorescence Lifetime Analysis of DNA Intercalated Ethidium Bromide and Quenching by Free Dye. *Biophys. Chem.* **1994**, *50*, 305–312. [[CrossRef](#)] [[PubMed](#)]
78. He, X.M.; Carter, D.C. Atomic Structure and Chemistry of Human Serum Albumin. *Nature* **1992**, *358*, 209–215. [[CrossRef](#)] [[PubMed](#)]
79. Olson, R.E.; Christ, D.D. Chapter 33. Plasma Protein Binding of Drugs. *Annu. Rep. Med. Chem.* **1996**, *31*, 327–336. [[CrossRef](#)]
80. Zhao, G.; Lin, H.; Zhu, S.; Sun, H.; Chen, Y. Dinuclear Palladium(II) Complexes Containing Two Monofunctional $[\text{Pd}(\text{En})(\text{Pyridine})\text{Cl}]^+$ Units Bridged by Se or S. Synthesis, Characterization, Cytotoxicity and Kinetic Studies of DNA-Binding. *J. Inorg. Biochem.* **1998**, *70*, 219–226. [[CrossRef](#)] [[PubMed](#)]
81. Stella, L.; Capodilupo, A.L.; Bietti, M. A Reassessment of the Association between Azulene and [60]Fullerene. Possible Pitfalls in the Determination of Binding Constants through Fluorescence Spectroscopy. *Chem. Commun.* **2008**, 4744–4746. [[CrossRef](#)] [[PubMed](#)]

82. Wu, S.S.; Yuan, W.B.; Wang, H.Y.; Zhang, Q.; Liu, M.; Yu, K.B. Synthesis, Crystal Structure and Interaction with DNA and HSA of (N,N'-Dibenzylethane-1,2-Diamine) Transition Metal Complexes. *J. Inorg. Biochem.* **2008**, *102*, 2026–2034. [[CrossRef](#)] [[PubMed](#)]
83. Selaković, S.; Rodić, M.V.; Novaković, I.; Matić, I.Z.; Stanojković, T.; Pirković, A.; Živković, L.; Spremo-Potparević, B.; Milčić, M.; Medaković, V.; et al. Cu(II) Complexes with a Salicylaldehyde Derivative and α -Diimines as Co-Ligands: Synthesis, Characterization, Biological Activity. Experimental and Theoretical Approach. *Dalton Trans.* **2024**, *53*, 2770–2788. [[CrossRef](#)] [[PubMed](#)]
84. Laitinen, O.H.; Hytönen, V.P.; Nordlund, H.R.; Kulomaa, M.S. Genetically Engineered Avidins and Streptavidins. *Cell. Mol. Life Sci.* **2006**, *63*, 2992–3017. [[CrossRef](#)]
85. Marmur, J. A Procedure for the Isolation of Deoxyribonucleic Acid from Micro-Organisms. *J. Mol. Biol.* **1961**, *3*, 208–218. [[CrossRef](#)]
86. Reichmann, M.E.; Rice, S.A.; Thomas, C.A.; Doty, P. A Further Examination of the Molecular Weight and Size of Desoxypentose Nucleic Acid. *J. Am. Chem. Soc.* **1954**, *76*, 3047–3053. [[CrossRef](#)]
87. Bruker Analytical X-ray Systems, Inc. *Apex2, Version 2 User Manual, M86-E01078*; Bruker Analytical X-ray Systems, Inc.: Billerica, MA, USA, 2006.
88. Siemens Industrial Automation, Inc. *SADABS: Area-Detector Absorption Correction*; Siemens Industrial Automation, Inc.: Madison, WI, USA, 1996.
89. Palatinus, L.; Chapuis, G. SUPERFLIP—A Computer Program for the Solution of Crystal Structures by Charge Flipping in Arbitrary Dimensions. *J. Appl. Crystallogr.* **2007**, *40*, 786–790. [[CrossRef](#)]
90. Betteridge, P.W.; Carruthers, J.R.; Cooper, R.I.; Prout, K.; Watkin, D.J. CRYSTALS Version 12: Software for Guided Crystal Structure Analysis. *J. Appl. Crystallogr.* **2003**, *36*, 1487. [[CrossRef](#)]

Disclaimer/Publisher's Note: The statements, opinions and data contained in all publications are solely those of the individual author(s) and contributor(s) and not of MDPI and/or the editor(s). MDPI and/or the editor(s) disclaim responsibility for any injury to people or property resulting from any ideas, methods, instructions or products referred to in the content.